Fibers and Polymers 2017, Vol.18, No.11, 2153-2160
DOI 10.1007/s12221-017-6944-y

ISSN 1229-9197 (print version)
ISSN 1875-0052 (electronic version)

Functionalized Graphene Nanoplatelets/Poly(ethylene oxide) Nanocomposites: Correlation between Crystallization Behavior and Mechanical Performance

Sepideh Gomari, Ismaeil Ghasemi*, and Masoud Esfandeh

Faculty of Processing, Iran Polymer and Petrochemical Institute, Tehran 14965/115, Iran
(Received September 24, 2016; Revised July 17, 2017; Accepted August 7, 2017)

Abstract: Poly(ethylene oxide) (PEO) nanocomposites containing pristine or functionalized graphene nanoplatelets (FGnP) prepared via solution blending and thermal and mechanical properties of nanocomposites were investigated. Chemical functionalization of graphene nanoplatelets was conducted through an amidation reaction between carboxylic acid groups of acidified graphene and hydroxyl groups of polyethylene glycol (PEG). An interfacial linkage and a good dispersion of FGnP was observed via scanning electron microscope (SEM). Differential scanning calorimetry (DSC) analysis revealed that the degree of crystallinity of samples decreased by addition of graphene nanoplatelets, while the size of spherulites increased as indicated by polarized optical microscope (POM). A lower degree of crystallinity and larger spherulites were detected in the case of FGnP. Filler/matrix interfacial adhesion was also remarkably influenced the mechanical properties of PEO as an effective reinforcement of matrix obtained upon the addition of FGnP nanosheets compared to untreated graphene.

Keywords: Poly(ethylene oxide), Graphene, Mechanical properties, Crystallization behavior, Solid polymer electrolytes

Introduction

Graphene nanoplatelets (GnP) are a new class of carbonaceous nanoparticles which have attracted great research interest, especially in polymer nanocomposites, since their discovery in 2004 [1-3]. These nanoplatelets which consists of a two-dimensional lattice of carbon atoms arranged in a honeycomb structure, are found to be the strongest material ever measured with Young's modulus of 1 TPa and strength of 130 GPa [4,5]. The enhancement in different properties of polymer can be obtained by addition of very low loadings of graphene just when a well-dispersed morphology of graphene inside the nanocomposite is achieved. It is recognized that exfoliation of graphene into thin or even single layer nanosheets needs a high interfacial adhesion between graphene and polymer chains. Pristine graphene establishes weak interfacial interaction with polar polymers, due to its hydrophobic nature. Hence, chemical functionalization of graphene, either through covalent [6,7] or non-covalent [8,9] methods is required. Non-covalent modification methods are usually used when high electrical conductivity is needed. However, in the case of enhanced mechanical properties, covalent methods are preferred [10]. This can be done by grafting of matrix-compatible groups onto graphene surface [11]. For example, Ren *et al.* [12] prepared dodecyl amine functionalized graphene by using amidation reaction and chemical reduction as a nanofiller for high-density polyethylene. Similarly, silane modification of exfoliated graphite was performed in order to increase the thermal conductivity and mechanical properties of epoxy matrix [13].

Poly(ethylene oxide) (PEO) is a hydrophilic semi-crystalline polymer with a wide range of applications such as host polymer in solid polymer electrolytes (SPEs) and biomedical uses [14-16]. In the last decade, many researches focused on PEO nanocomposites showed that they have higher ionic conductivity and better mechanical properties in comparison to neat PEO [17-20]. As explained above, a good dispersion state of graphene provides the advantage of large surface area per unit volume of these nanoplatelets, therefore, it could highly affect the thermal and mechanical properties of the matrix [21]. The effect of organically modified clay on the thermomechanical properties of PEO was evaluated by Ratna et. al. The highest mechanical properties was obtained at the clay content of 12.5 wt.% and the crystallinity of nanocomposites showed a reduction [22]. Yang *et al.* incorporated phenoxy-grafted multiwalled carbon nanotubes into PEO and studied the mechanical properties of nanocomposites [6]. By addition of 1.5 wt.% of nanotubes a remarkable increase in Young's modulus, tensile strength, ultimate strain and toughness of PEO was obtained, while no significant effect on the crystallization properties was detected. Mahmoud [23] compared melt blending and solvent mixing preparation methods of PEO/thermally reduced graphene nanocomposites and showed that the solvent blended sample indicates higher mechanical performance compared to melt compounded. However, the elongation at break of samples decreased upon the increasing in graphene concentration.

Since modifying the interfacial interactions at the nanoparticles surface considered as a route to change the different properties of materials, this has motivated us to study the effect of graphene functionalization on thermo-mechanical properties of PEO. In this work, two different kinds of graphene were used including pure graphene and chemically modified graphene with polyethylene glycol (PEG). This was accomplished by the esterification reaction of carboxylic acid groups of oxidized graphene with hydroxyl groups of PEG. Polymer nanocomposites were prepared using solvent

*Corresponding author: i.ghasemi@ippi.ac.ir

blending method and morphological, thermal and mechanical properties were fully characterized. The interrelationship between nanocomposite morphology and properties will be emphasized.

Experimental

Materials

Graphene nanoplatelets of grade C750 supplied from XG Sciences (USA) with a thickness of 1-5 nm. PEO with a molecular weight of 900,000 g/mol was obtained from Scientific Polymer Products, Inc. (Ontario, NY). PEG (400 g/mol) received from Sigma-Aldrich. Acetonitrile solvent, nitric acid and sulfuric acid as oxidizing agents and N,N-dicyclohexylcarbodiimide (DCC) as the condensing agent were purchased from Merck (Germany).

Chemical Functionalization of GnP

GnP was mixed with a 1:1 v/v mixture of H_2SO_4 (8 M) and HNO_3 (8 M) by vigorous stirring for 15 min and then bath sonicated at 60 °C for 2 hr to prepare carboxylic acid functionalized graphene (GnP-COOH). The obtained mixture was diluted with deionized water and the solid residue was repeatedly washed with deionized water by decantation and centrifugation. Finally, the product was dried under vacuum at 60 °C for 24 hr.

In order to graft PEG to the graphene surface, a procedure reported in the literature with slight modifications was used [24]. 0.5 gr of GnP-COOH nanoplatelets was mixed with 2 gr PEG400 and 0.05 gr dried DCC in 40 m*l* of anhydrous tetrahydrofuran (THF) under N_2 atmosphere. The mixture was reacted for 48 hr at 60 °C while vigorously stirring under reflux and N_2 atmosphere. After reaction completion, the suspension was filtered and washed several times with absolute ethanol and deionized water to remove the unreacted PEG. PEG grafted graphene (FGnP) was acquired after drying the solid residue at 60 °C under vacuum for 24 hr.

Preparation of Nanocomposite Samples

A certain amount of dried GnP (or FGnP) was dispersed in acetonitrile (1 mg/m*l*) by magnetic stirring overnight and then by bath sonicating for 3 hr. FGnP dispersion was gradually added to a clear solution of PEO/acetonitrile and stirred for 24 hr at 50 °C. Afterwards, the mixture was poured into glass petri dishes and dried firstly at room temperature and secondly at 40 °C under vacuum to eliminate any traces of solvent. The prepared nanocomposites labeled as PEO/GnP and PEO/FGnP, containing 0.1 and 1 wt.% of GnP or FGnP, respectively.

Characterization

Fourier transform infrared spectra were obtained with a Bruker EQUINOX 55 FT-IR spectrometer. Morphology of nanocomposites was investigated using a scanning electron microscopy (SEM) on a Tescan VEGA-II SEM, equipped with energy dispersive X-ray analysis (EDX). Thermogravimetric analysis was carried out on a TGA/DSC1 Mettler Toledo (Switzerland) from room temperature to 700 °C under nitrogen atmosphere at a heating rate of 10 °C/min. X-ray diffraction (XRD) patterns was obtained on Siemens D5000, Germany, using Cu Kα radiation source (λ=0.154 nm) at 40 kV and 40 mA. The degree of crystallinity was determined using the following equation [25]:

$$\%X_c = \frac{\text{Area of the crystalline peaks}}{\text{Total area (crystalline and amorphous)}} \times 100 \quad (1)$$

Differential scanning calorimetry analysis was conducted using a DSC1 Mettler Toledo (Switzerland) differential scanning calorimeter. The heating/cooling experiments were performed under N_2 atmosphere with a rate of 10 °C/min. In order to erase the thermal history, each sample was heated to 100 °C and kept for 10 minutes. The crystalline morphology and spherulitic structure of samples were observed by means of a Carl Zeiss Jena JENAPOL polarized optical microscope (POM). All samples were melted at 120 °C for 10 min to remove thermal history and then naturally cooled to room temperature before testing. The stress-strain behavior of the nanocomposites was measured according to ASTM D882 on a universal testing machine (STM-20, SANTAM, Iran) with a strain rate of 40 mm/min. The sample dimensions were 5 mm×25 mm with a thickness of 100-200 μm.

Results and Discussion

Characterization of FGnP Nanosheets

Pristine graphene sheets are hydrophobic and tend to form aggregations through van der Waals interactions especially in hydrophilic solvents and polymers. The formation of aggregates can be prevented by chemical modification and attachment of some molecules or polymers onto the sheets. Since PEG has the same structure as PEO, it is expected to establish good interactions between PEG grafted graphene and PEO. Different methods were employed for the identification and assessment of functionalization reactions, including FT-IR spectroscopy, EDX analysis and TGA. The FT-IR spectra of pristine GnP, GnP-COOH, FGnP and pure PEG400 are presented in Figure 1. GnP-COOH exhibited a new peak at 1712 cm^{-1} related to the stretching vibration of carbonyl groups (C=O). In addition, OH hydroxyl groups showed a strong band at around 3443 cm^{-1}. These two peaks suggesting the presence of carboxylic acid groups on the graphene sheets which have also been reported in the literature [26,27]. In the FT-IR spectrum of FGnP sample a new peak appeared at 1102 cm^{-1}, attributed to C-O-C ether groups of PEG. The formation of ester linkages has been confirmed through the blue shift of carbonyl band to 1746 cm^{-1} [28]. Furthermore, the intensity of hydroxyl absorption band of PEG end groups (at 3443 cm^{-1}) and C-H

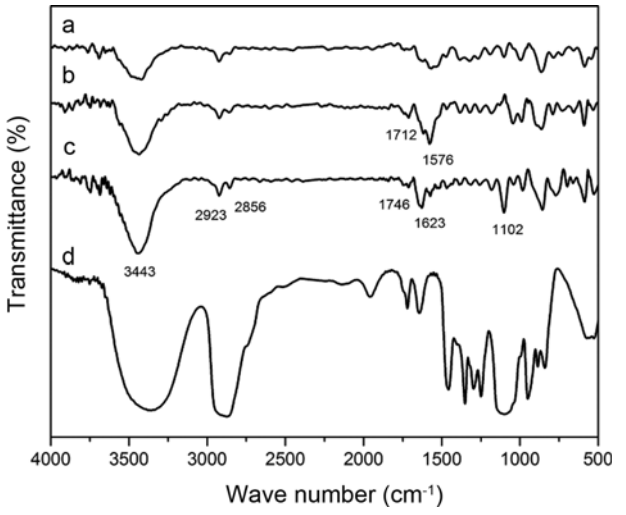

Figure 1. FT-IR spectra of (a) GnP, (b) GnP-COOH, (c) FGnP and (d) PEG400.

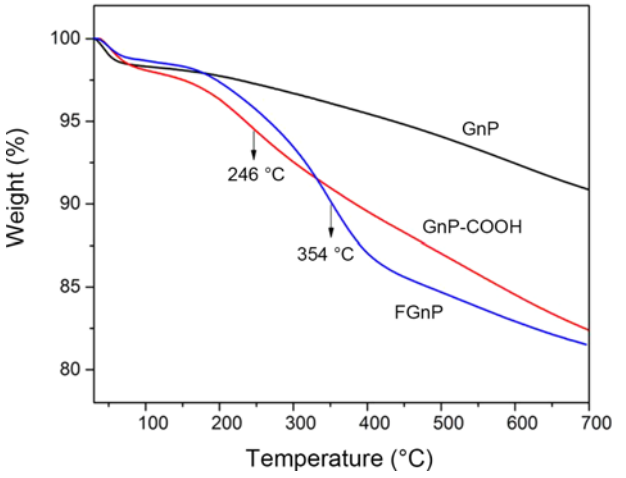

Figure 2. TGA curves of GnP, GnP-COOH and FGnP at a heating rate of 10 °C/min.

Table 1. EDX chemical composition of pristine and functionalized graphene nanoplatelets

	GnP	GnP-COOH	FGnP
Carbon (wt.%)	97.9	89.4	85.7
Oxygen (wt.%)	2.1	10.6	14.3
O/C ratio	0.021	0.118	0.167

stretching of alkyl groups of PEG (at 2856 and 2932 cm^{-1}) has been enhanced. Together, these observations demonstrate the successful chemical grafting of PEG onto graphene nanosheets.

In order to specify the main elements concentration, EDX analysis was conducted on GnP, GnP-COOH and FGnP samples and the results were reported in Table 1. Acid treatment on GnP has raised the amount of oxygen atom from 2.1 to 10.6 wt.% for GnP-COOH sample. After functionalization with PEG, the oxygen concentration reached 14.3 wt.% value for FGnP. Therefore, the increment of oxygen atom content and its ratio to carbon element verify that the oxidation reaction and grafting of PEG has proceeded effectively.

TGA was used to evaluate the content of oxidized groups on GnP-COOH and PEG molecules grafted onto FGnP. As seen in Figure 2, all samples show a weight loss around 100 °C which is related to the removal of physically adsorbed water. The gradual weight loss of GnP could be attributed to the degradation of some organic groups present on the surface. For the GnP-COOH, a second weight loss of 6.5 % was detected around 246 °C ascribed to the pyrolysis of the carboxylic functional groups [27,29]. In the FGnP curve, a weight loss of 13 % with a maximum weight loss rate at 354 °C was found due to PEG molecules decomposition [24,30]. This implies that the content of PEG chains grafted on FGnP can be estimated as 13 wt.% which is higher than oxygenated groups' content in GnP-COOH as it is expected because of higher molecular weight of PEG (400 g/mol).

Morphology of Nanocomposites

SEM micrographs of fractured surface of PEO nanocomposites containing pristine and functionalized graphene are illustrated in Figure 3. From Figures 3(a) and 3(b), some aggregation of graphene nanoplatelets can be observed in PEO/GnP nanocomposites, especially in higher contents of

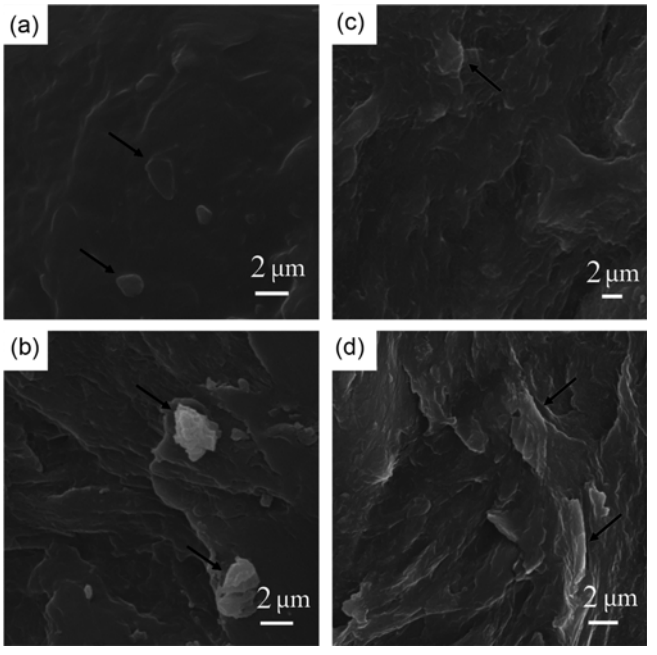

Figure 3. SEM micrographs of (a) PEO/GnP0.1, (b) PEO/GnP1, (c) PEO/FGnP0.1, and (d) PEO/FGnP1.

Gnp (1 wt.%). In addition, no substantial adhesion between graphene surface and PEO matrix could be detected. This is an indication of weak interactions between PEO and pristine graphene. In contrast, no visible agglomerations were found in PEO/FGnP nanocomposites in Figures 3(c) and 3(d). Another interesting point is that a strong adhesion at the interface of FGnP and polymer matrix was discovered, meaning that grafting of PEG molecules which have a good miscibility with PEO, enhanced the compatibility between graphene surface and PEO chains. Therefore, a homogeneous dispersion of FGnP nanosheets was obtained in the PEO/FGnP nanocomposites.

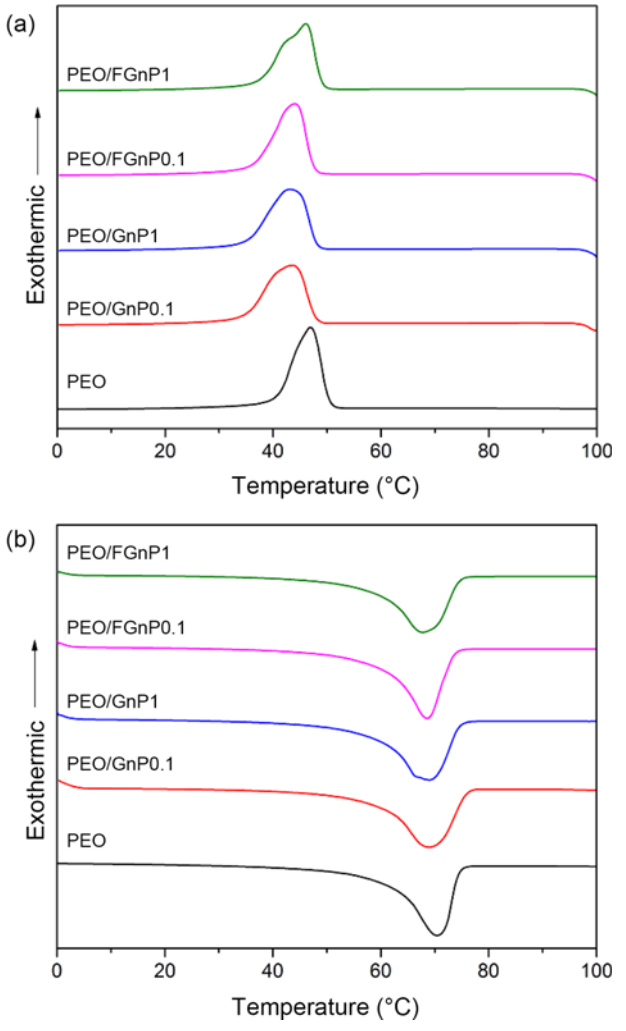

Figure 4. DSC traces of neat PEO and nanocomposites containing 0.1 and 1 wt.% of pristine and functionalized graphene; (a) cooling and (b) second heating.

Thermal Properties

The crystallization behavior of PEO with and without graphene nanoplatelets was studied using DSC analysis. The nanocomposite samples with various contents of GnP or FGnP were subjected to DSC analysis and the cooling/heating traces are shown in Figure 4. Some useful data that can be extracted from these curves such as the onset crystallization temperature (T_{onset}), the peak crystallization temperature (T_c), the degree of supercooling ($\Delta T=T_{onset}-T_c$), full width at the half height maximum of the crystallization peak (FWHM), enthalpy of crystallization (ΔH_c), melting temperature (T_m), enthalpy of melting (ΔH_m) and degree of crystallinity (X_c) are listed in Table 2. The incorporation of graphene nanoplatelets into PEO matrix seems to have a considerable effect on the crystallization exotherm peak and melting behavior. As can be seen in Figure 4(a), the crystallization temperature (T_c) reduced by addition of GnP and FGnP into neat PEO. This means that these nanoplatelets act as anti-nucleating agents to hinder the PEO crystallization. Although nanoparticles generally act as heterogeneous nucleating agents in a polymeric matrix [31,32], incorporation of fillers into PEO leads to a different crystallization behavior as reported by many researchers [33-35].

It is noticed from Table 2 that ΔH_c reduced with the addition of graphene, especially the functionalized ones. Strong interactions between PEG grafted graphene and PEO chains provide a fine dispersion of graphene sheets, which in turn disturbs the polymeric chains order to form crystalline structures. Similar observations were reported by the addition of modified carbon nanotube into PEO [36]. ΔT which implies to the crystallization rate, has higher values in PEO/GnP and PEO/FGnP nanocomposites in comparison to neat

Table 2. DSC analysis data for PEO and PEO/graphene nanocomposites

Sample		PEO	PEO/GnP0.1	PEO/GnP1	PEO/FGnP0.1	PEO/FGnP1
Cooling	T_{onset} (°C)	50.51	47.54	48.08	47.92	49.14
	T_c (°C)	46.97	43.55	45.22	44.02	45.10
	ΔT	3.54	4.99	3.86	3.90	4.04
	ΔH_c (J/g)	129.72	127.80	127.86	126.90	126.84
	FWHM (°C)	5.88	8.42	8.24	6.55	7.20
Second heating	T_m (°C)	70.42	68.71	68.99	68.60	67.52
	ΔH_m (J/g)	144.90	136.44	138.60	129.00	128.64
	X_c (%)	67.81	63.85	64.86	60.36	60.20

sample. Therefore, it can be understood that it is more difficult for PEO chains to crystallize in the presence of graphene nanosheets. FWHM is considered as an indication of the spherulites size distribution, so the smaller FWHM values demonstrate narrower size distribution. In the PEO/GnP and PEO/FGnP nanocomposites, FWHM was greater than that of neat PEO. This means that GnP or FGnP addition broadens the distribution of spherulites size.

According to Figure 4(b) and Table 2, the values of T_m, ΔH_m and X_c reduced after addition of GnP and a further reduction was observed by FGnP incorporation. X_c was calculated using equation: $X_c=\Delta H_m/\Delta H_m^o\times100$ %, where ΔH_m is the melting enthalpy of sample and ΔH_m^o is the melting enthalpy of 100 % crystalline PEO which is equal to 213.7 J/g [37]. A higher reduction of PEO crystallinity in the presence of FGnP can be ascribed to better dispersion of these nanosheets and stronger interactions with polymer chains which hinder chain folding and formation of crystallites.

Polarized optical microscopy was conducted with the objective of giving an insight into spherulitic morphology of PEO in the presence of pristine and modified graphene and illustrated in Figure 5. A "Maltese-cross" extinction pattern [38], with average spherulites diameter of ~230 μm was observed for PEO in Figure 5(a). After addition of FGnP, a reduction in nucleation sites and an increment in spherulites diameter was distinguished, as the average spherulite diameter of 400 and 590 μm was evaluated for PEO/FGnP0.1 (Figure 5(d)) and PEO/FGnP1 (Figure 5(e)), respectively. This confirms the anti-nucleating effect of graphene nanosheets to suppress the crystallization of PEO which was anticipated from T_c measurements. Likewise, a gradual growth of spherulites size was disclosed for PEO/GnP nanocomposites, where spherulites with average diameter of 250 and 260 μm was formed by addition of 0.1 wt% of GnP (Figure 5(b)) and 1 wt.% of GnP (Figure 5(c)), respectively. By comparison of spherulites size and the number of nucleation sites in

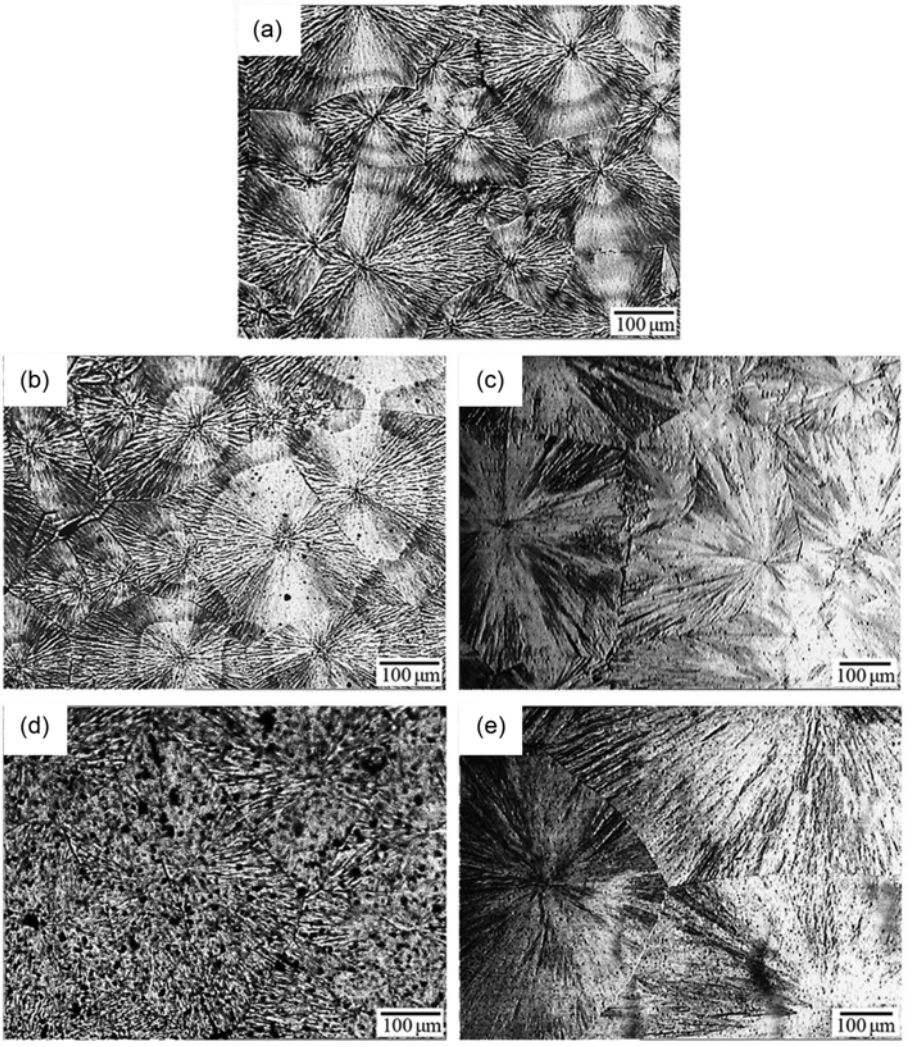

Figure 5. POM images of (a) PEO, (b) PEO/GnP0.1, (c) PEO/GnP1, (d) PEO/FGnP0.1, and (e) PEO/FGnP1.

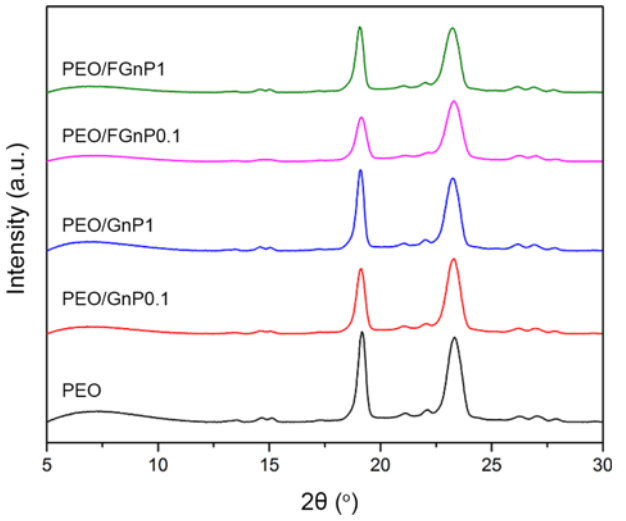

Figure 6. XRD patterns of PEO and PEO/graphene nanocomposites.

nanocomposites, it can be concluded that FGnP nanosheets more significantly change the crystalline structure of PEO. The increase of spherulites dimension upon the addition of nanoparticles was also reported by other researchers [33,36]. Furthermore, POM images of PEO/GnP nanocomposites evidently shows stacks of graphene sheets especially at 1 wt.% concentration, while a homogeneous dispersion of FGnP confirm the existence of suitable interactions with PEO chains.

A typical X-ray diffraction (XRD) of neat PEO and nanocomposite samples indicated in Figure 6 to elucidate the effect of interfacial interactions and different compositions on crystalline structure. All samples show two characteristic peaks of crystalline PEO at 2θ=19.2 ° and 23.4 °, which are assigned to (120) and (112) planes, respectively [39]. However, the intensity of peaks decreases after addition of graphene nanoplatelets and remarkably the functionalized ones. The degree of crystallinity of samples based on the XRD method was calculated according to equation (1) and the results are reported in Table 3. Nanocomposite samples indicated lower degree of crystallinity compared to neat PEO. It is notable that PEO/FGnP samples showed lower crystallinity as was also discovered by DSC analysis. These findings suggest that the stronger interactions between FGnP and PEO chains may be responsible for restricting the polymer crystallization. It seems that at lower contents of graphene nanoplatelets, a lower degree of crystallinity was obtained. It could be related to a better dispersion of graphene nanoplatelets at 0.1 wt.% which was confirmed from SEM images. Generally, In the XRD patterns of graphene nanoplatelets a peak appears at 2θ=26.3 ° [3]. Nevertheless, no characteristic peak of graphene was observed in the XRD patterns of PEO nanocomposites. It may be related to the low concentration of graphene nanoplatelets and probable overlapping with weak peaks of pure PEO around 2θ=26.3 ° and 27 ° [17,40] in the samples.

Table 3. Degree of crystallinity of samples based on XRD

Sample	Degree of crystallinity (%)
PEO	80.5
PEO/GnP0.1	76.7
PEO/GnP1	77.4
PEO/FGnP0.1	73.9
PEO/FGnP1	74.6

Mechanical Properties

The tensile stress-elongation curves for PEO and its nanocomposites are represented in Figure 7 and the results are summarized in Table 4. The elongation at break of PEO (639.7 %) was significantly increased by addition of just 0.1 wt.% of graphene in both PEO/GnP and PEO/FGnP nanocomposites. Since at low content of graphene, there is no large difference between the dispersion state of these nanoplatelets and the extent of agglomerations in the case of GnP is not very high, a considerable difference between mechanical performance of PEO/GnP0.1 and PEO/FGnP0.1 cannot be observed in spite of the strong interfacial adhesion between FGnP and PEO. As the FGnP content was increased from 0.1 to 1 wt.%, a further increase in the elongation at break was observed from 1010.3 % to 1720.8 %. However, it was reduced from 1311.8 % to 1130.1 % as the GnP content increased from 0.1 to 1 wt.%. This may arise from the high degree of agglomerations for GnP nanosheets as detected in SEM micrographs and POM images. These agglomerations and weak interfacial interactions could act as stress concentrators to facilitate the craze formation and

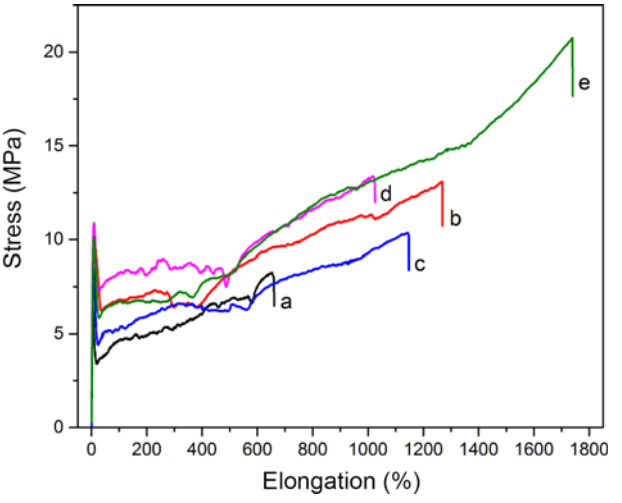

Figure 7. Tensile stress-elongation curves of neat PEO and its nanocomposites; (a) PEO, (b) PEO/GnP0.1, (c) PEO/GnP1, (d) PEO/FGnP0.1, and (e) PEO/FGnP1.

Table 4. Tensile properties of neat PEO and its nanocomposites with pristine and functionalized graphene

Sample	PEO	PEO/GnP0.1	PEO/GnP1	PEO/FGnP0.1	PEO/FGnP1
Young's modulus (MPa)	207.0±7.2	301.6±26	307.1±27.7	329.3±43	342.4±11
Yield stress (MPa)	6.8±0.45	10.8±1.11	8.97±0.93	10.66±0.21	10.48±0.35
Tensile strength (MPa)	7.83±0.43	15.24±1.08	10.13±1.04	15.87±0.63	19.38±1.06
Toughness (MJ/m^3)	33.4±4.6	140.8±23.7	88.7±7.6	129.4±3.8	188.9±14.2
Elongation at break (%)	602.1±58	1311.8±35	1130.1±67	1010.3±82	1720.8±20

deteriorate the mechanical performance of nanocomposite. From Table 4 it is obvious that Young's modulus, tensile strength and toughness of PEO were also improved by incorporation of fillers. Interestingly, PEO/FGnP nanocomposites display markedly higher mechanical properties in comparison to PEO/GnP. For instance, the Young's modulus of nanocomposites containing 1 wt.% of nanoplatelets increased by 65 % for FGnP against 48 % for GnP, tensile strength increased by 148 % for FGnP versus 29 % for GnP, and toughness increased by 466 % for FGnP versus 165 % for GnP. Tensile strength and toughness of PEO/FGnP nanocomposites showed an increasing trend with the addition of FGnP concentration. On the other hand, in PEO/GnP nanocomposites these parameters were increased by addition of 0.1 wt.% of GnP and then decreased at 1 wt.%.

It has been acknowledged that the mechanical reinforcement in polymer nanocomposites could be achieved if the following conditions were obtained: (i) a well dispersion state of nanoparticles in the polymeric matrix, and (ii) a strong interfacial adhesion between nanoparticles and polymer chains [41]. A good dispersion and exfoliation of graphene into thin sheets or even single sheets ensures benefit from large specific area of these nanoparticles in the polymer matrix. Moreover, strong interfacial interactions provide an efficient load transfer from surrounding matrix into graphene nanoplatelets [42]. This can be used to explain the effect of functionalization and interfacial interactions on the mechanical properties of nanocomposites, particularly on tensile strength. The hydroxyl end groups of PEG grafted onto graphene nanosheets are supposed to establish strong hydrogen bonds with ether oxygen atoms of PEO backbone [43]. As mentioned previously, SEM images confirmed the existence of strong adhesion between FGnP and PEO, while a poor interaction between GnP and PEO was observed. Thus, a greater enhancement in mechanical properties of nanocomposite is expectable by addition of FGnP to PEO matrix compared to unmodified GnP.

It is notable that, another factor which affects the mechanical properties in semi-crystalline polymers is the degree of crystallization. Indeed, a higher degree of crystalline phases could increase the stiffness and strength of sample due to the reinforcing effect of crystallites [31,44,45]. DSC investigations revealed that graphene incorporation does not have an increasing effect on the degree of crystallization of PEO. However, the degree of crystallization decreased by ~3 % after GnP and ~7 % after FGnP and addition. Consequently, the large aspect ratio of graphene and its high intrinsic mechanical properties in combination with enhanced adhesion interactions in the case of FGnP, contribute in the improvement of mechanical performance of PEO nanocomposites.

Conclusion

Nanocomposites based on PEO and different concentrations of graphene nanoplatelets (pristine and functionalized) were prepared via solution blending method. Functionalization of graphene with PEG provided an enhanced interfacial adhesion and a homogenous dispersion of these nanosheets through the matrix in comparison to pristine graphene. POM images revealed the anti-nucleating effect of graphene as the nucleation density reduced in PEO/GnP and PEO/FGnP nanocomposites. A lower degree of crystallinity was determined for nanocomposites and especially PEO/FGnP nanocomposites using DSC analysis and XRD patterns. The compact molecular packing and crystallization of PEO was significantly influenced and disturbed by FGnP loading due to the existence of interactions between ether oxygen atoms of PEO with PEG chains grafted onto graphene. A remarkable enhancement in mechanical performance of PEO was observed by incorporation of FGnP nanosheets and in higher concentration. As a result, PEO/FGnP1 sample exhibited the maximum elongation at break, Young's modulus, tensile strength and toughness increased by 186, 65, 148 and 466 %, respectively, in comparison to neat PEO. Thus it can be concluded that by enhancing the interfacial interactions between graphene nanosheets and PEO matrix, it is possible to concurrently increase the stiffness and toughness of PEO.

Acknowledgements

We gratefully acknowledge financial support from the Iranian National Science Foundation (INSF, Grant No. 94013014).

References

1. K. S. Novoselov, A. K. Geim, S. V Morozov, D. Jiang, Y. Zhang, S. V Dubonos, I. V Grigorieva, and A. A. Firsov,

Science, **306**, 666 (2004).
2. J. R. Potts, D. R. Dreyer, C. W. Bielawski, and R. S. Ruoff, *Polymer*, **52**, 5 (2011).
3. H. Kim, A. A. Abdala, and C. W. Macosko, *Macromolecules* **43**, 6515 (2010).
4. T. Kuilla, S. Bhadra, D. Yao, N. Hoon, S. Bose, and J. Hee, *Prog. Polym. Sci.,* **35**, 1350 (2010).
5. C. Lee, X. Wei, J. W. Kysar, and J. Hone, *Science,* **321**, 385 (2008).
6. B.-X. Yang, J.-H. Shi, K. P. Pramoda, and S. H. Goh, *Nanotechnology,* **18**, 125606 (2007).
7. S. Stankovich, R. D. Piner, S. T. Nguyen, and R. S. Ruoff, *Carbon,* **44**, 3342 (2006).
8. H. B. Lee, A. V Raghu, K. S. Yoon, and H. M. Jeong, *J. Macromol. Sci. Part B* **49**, 802 (2010).
9. J. Liu, W. Yang, L. Tao, D. Li, C. Boyer, and T. P. Davis, *J. Polym. Sci. Part A Polym. Chem.,* **48**, 425 (2010).
10. J. Liu, J. Tang, and J. J. Gooding, *J. Mater. Chem*., **22**, 12435 (2012).
11. J. Lee, K. E. Su, E. P. Chan, Q. Zhang, T. Emrick, and A. J. Crosby, *Macromolecules*, **40**, 7755 (2007).
12. P. Ren, H. Wang, H. Huang, D. Yan, and Z. Li, *J. Appl. Polym. Sci.,* **131**, 39803 (2013).
13. S. Ganguli, A. K. Roy, and D. P. Anderson, *Carbon,* **46**, 806 (2008).
14. A. Magistris and C. Fisica, *Polym. Int.,* **28**, 277 (1992).
15. B. Scrosati and C. A. Vincent, *MRS Bull.,* **25**, 28 (2000).
16. S. Dhawan, K. Dhawan, M. Varma, and V. R. Sinha, *Pharm. Technol*., **29**, 82 (2005).
17. C. Shen, J. Wang, Z. Tang, H. Wang, H. Lian, J. Zhang, and C. Cao, *Electrochim. Acta,* **54**, 3490 (2009).
18. D. Zhou, X. Mei, and J. Ouyang, *J. Phys. Chem. C*, **115**, 16688 (2011).
19. M. Yuan, J. Erdman, C. Tang, and H. Ardebili, *RSC Adv*., **4**, 59637 (2014).
20. S. L. Agrawal, M. Singh, M. M. Dwivedi, and K. Pandey, *Fiber. Polym*., **12**, 864 (2011).
21. T. Ramanathan, A. A. Abdala, S. Stankovich, D. A. Dikin, R. D. Piner, D. H. Adamson, H. C. Schniepp, X. Chen, R. S. Ruoff, S. T. Nguyen, I. A. Aksay, R. K. P. Homme, and L. C. Brinson, *Nat. Nanotechnol.*, **3**, 327 (2008).
22. D. Ratna, S. Divekar, A. B. Samui, B. C. Chakraborty, and A. K. Banthia, *Polymer (Guildf)*, **47**, 4068 (2006).
23. W. E. Mahmoud, *Eur. Polym. J*., **47**, 1534 (2011).
24. L. Niu, Y. Luo, and Z. Li, *Sensors Actuators B Chem*., **126**, 361 (2007).
25. J. F. Rabek, "Experimental Methods in Polymer Chemistry: Physical Principles and Application", pp.436-478, Wiley, 1980.
26. S. Zhang, P. Xiong, X. Yang, and X. Wang, *Nanoscale*, **3**, 2169 (2011).
27. H. Kuo, F. Cheng, N. G. Sahoo, Y. P. Tan, Y. Pan, H. Bao, L. Li, S. H. Chan, and J. Zhao, *ACS Appl. Mater. Interfaces,* **4**, 2387 (2012).
28. G. Socrates, *Infrared and Raman Characteristic Group Frequencies: Tables and Charts",* John Wiley & Sons, 2004.
29. S. Niyogi, E. Bekyarova, M. E. Itkis, J. L. McWilliams, M. A. Hamon, and R. C. Haddon, *J. Am. Chem. Soc.,* **128**, 7720 (2006).
30. S. Han, C. Kim, and D. Kwon, *Polymer,* **38**, 317 (1997).
31. M. El Achaby, F. Arrakhiz, S. Vaudreuil, A. el Kacem Qaiss, M. Bousmina, and O. Fassi-Fehri, *Polym. Compos*., **33**, 733 (2012).
32. J. Y. Kim, H. S. Park, and S. H. Kim, *Polymer,* **47**, 1379 (2006).
33. N. Rahmansyah, C. Lo, C. Syu, and C. Lee, *J. Appl. Polym. Sci*., **122**, 1236 (2011).
34. A. Adhikari and K. Lozano, *J. Polym. Res*., **18**, 875 (2011).
35. T. Chatterjee, A. T. Lorenzo, and R. Krishnamoorti, *Polymer,* **52**, 4938 (2011).
36. J. Jin, M. Song, and F. Pan, *Thermochim. Acta,* **456**, 25 (2007).
37. X. Li and S. L. Hsu, *J. Polym. Sci. Polym. Phys. Ed*., **22**, 1331 (1984).
38. B.-K. Choi, *Solid State Ionics,* **168**, 123 (2004).
39. A. Dey, S. Karan, A. Dey, and S. K. De, *Mater. Res. Bull.,* **46**, 2009 (2011).
40. S. Gao, J. Zhong, G. Xue, and B. Wang, *J. Memb. Sci*., **470**, 316 (2014).
41. F. H. Gojny and K. Schulte, *Compos. Sci. Technol.*, **64**, 2303 (2004).
42. S.-Y. Fu, X.-Q. Feng, B. Lauke, and Y.-W. Mai, *Compos. Part B Eng*., **39**, 933 (2008).
43. F. Xiang, S. M. Ward, T. M. Givens, and J. C. Grunlan, *Soft Matter*, **11**, 1001 (2015).
44. K. E. Prasad, B. Das, U. Maitra, U. Ramamurty, and C. N. R. Rao, *Proc. Natl. Acad. Sci.*, **106**, 13186 (2009).
45. K. M. Seven, J. M. Cogen, and J. F. Gilchrist, *Polym. Eng. Sci*., **56**, 541 (2016).